LETTER

doi:10.1038/nature12485

A disinhibitory microcircuit initiates critical-period plasticity in the visual cortex

Sandra J. Kuhlman[1]†*, Nicholas D. Olivas[2]*, Elaine Tring[1], Taruna Ikrar[2], Xiangmin Xu[2,3] & Joshua T. Trachtenberg[1]

Early sensory experience instructs the maturation of neural circuitry in the cortex[1,2]. This has been studied extensively in the primary visual cortex, in which loss of vision to one eye permanently degrades cortical responsiveness to that eye[3,4], a phenomenon known as ocular dominance plasticity (ODP). Cortical inhibition mediates this process[4–6], but the precise role of specific classes of inhibitory neurons in ODP is controversial. Here we report that evoked firing rates of binocular excitatory neurons in the primary visual cortex immediately drop by half when vision is restricted to one eye, but gradually return to normal over the following twenty-four hours, despite the fact that vision remains restricted to one eye. This restoration of binocular-like excitatory firing rates after monocular deprivation results from a rapid, although transient, reduction in the firing rates of fast-spiking, parvalbumin-positive (PV) interneurons, which in turn can be attributed to a decrease in local excitatory circuit input onto PV interneurons. This reduction in PV-cell-evoked responses after monocular lid suture is restricted to the critical period for ODP and appears to be necessary for subsequent shifts in excitatory ODP. Pharmacologically enhancing inhibition at the time of sight deprivation blocks ODP and, conversely, pharmacogenetic reduction of PV cell firing rates can extend the critical period for ODP. These findings define the microcircuit changes initiating competitive plasticity during critical periods of cortical development. Moreover, they show that the restoration of evoked firing rates of layer 2/3 pyramidal neurons by PV-specific disinhibition is a key step in the progression of ODP.

Throughout the neocortex, form and function of neural circuitry are shaped by experience[1,2,7,8]. This sensitivity to experience is most pronounced during adolescence, and has been studied most extensively in the primary visual cortex[3,9], in which occluding vision through one eye (monocular deprivation; MD) results in cortical blindness to this eye, even after normal vision is restored[3,10–12]. With the goal of identifying the initial changes in cortical function after MD we used loose cell-attached recordings to isolate visually evoked responses from single neurons in binocular visual cortex in alert mice (Fig. 1a).

Unexpectedly, we found that visually evoked responses of excitatory pyramidal (PYR) neurons in layer (L)2/3 1 day after contralateral MD were roughly twice as strong as those in control mice. Evoked firing rates to stimulation through the ipsilateral eye, which had not been deprived, were approximately twofold higher than in controls (Fig. 1b, c; MD: 2.9 ± 0.4 Hz, control: 1.5 ± 0.4 Hz; one-way analysis of variance (ANOVA) $P = 0.028$, followed by post-hoc comparison, Tamhane corrected P value $P = 0.046$). Indeed, firing rates evoked by monocular viewing through the open eye after 1 day of MD were sufficiently increased

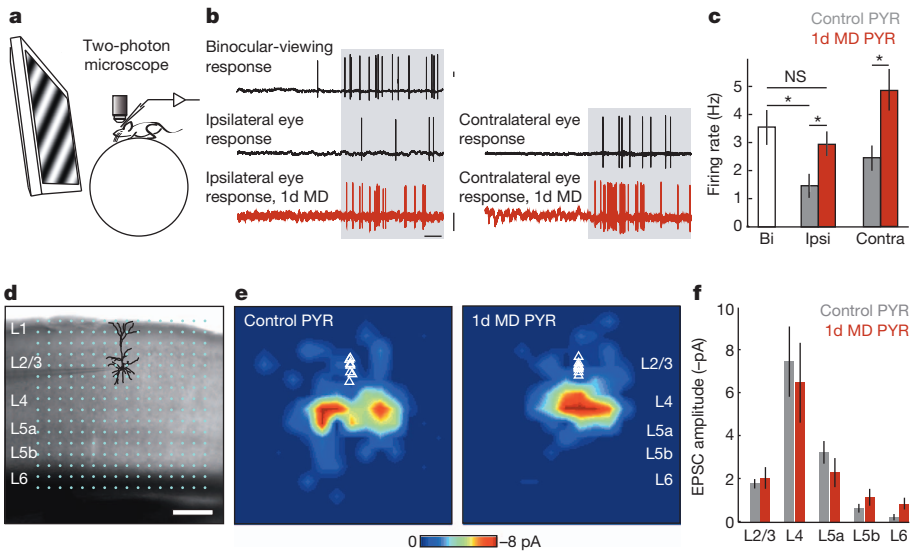

Figure 1 | L2/3 pyramidal neuron responsiveness and local circuit organization is unchanged 1 day after MD. **a**–**c**, Responses of PYR neurons to drifting gratings in alert mice. **a**, Cartoon of head-fixed configuration. **b**, Example loose cell-attached recordings from controls (black) and after 1-day (1d) MD (red) in response to visual stimulation (grey shading). Scale bar, 1 mV, 500 ms. **c**, Mean firing rate at optimal orientation (binocular (bi): 10 mice, $n = 30$ cells; ipsilateral (ipsi) control: 7 mice, $n = 22$ cells; ipsilateral MD: 6 mice, $n = 33$ cells; contralateral (contra) control: 3 mice, $n = 9$ cells; contralateral MD: 3 mice, $n = 10$ cells). **d**, PYR neuron recorded in binocular V1 in an acute slice; overlaid are 16 × 16 LSPS stimulation locations spanning pia to white matter. Scale bar, 200 μm. **e**, *In vitro* LSPS aggregate excitatory input maps pooled across PYR neurons. Triangles indicate soma location (control: 4 mice, $n = 9$ cells; MD: 4 mice, $n = 9$ cells). **f**, Mean LSPS-evoked EPSC amplitude, same cells as **e**. NS, not significant. *$P < 0.05$.

[1]Department of Neurobiology, David Geffen School of Medicine, University of California, Los Angeles, California 90048, USA. [2]Department of Anatomy and Neurobiology, University of California, Irvine, California 92697, USA. [3]Department of Biomedical Engineering, University of California, Irvine, California 92697, USA. †Present address: Department of Biological Sciences and the Center for the Neural Basis of Cognition, Carnegie Mellon University, Pittsburgh, Pennsylvania 15213, USA.
*These authors contributed equally to this work.

that they were indistinguishable from firing rates evoked during binocular viewing conditions in controls (Fig. 1b, c; binocular: 3.5 ± 0.6 Hz; Tamhane corrected *P* value $P = 0.834$). A doubling in excitatory firing rates was also seen when we acutely reopened the deprived contralateral eye and recorded responses to visual stimulation while shuttering the ipsilateral eye (Fig. 1b, c; MD: 4.8 ± 0.7 Hz, control: 2.4 ± 0.4 Hz; Mann–Whitney *U*-test $P = 0.02$). Notably, neurons were not responsive to stimulation through the sutured contralateral eye in alert mice. These findings show that following an immediate drop in visually evoked firing rates after MD (because responses are now only driven through one eye), evoked firing rates of PYR neurons are restored as cortical responsiveness to vision through the open eye increases. Thus, after 1 day of MD the firing rates of PYR neurons in L2/3 of the binocular visual cortex in alert mice that are viewing a scene with only one eye are roughly equivalent to firing rates in normal mice viewing a scene with both eyes.

The increased responsiveness of L2/3 PYR neurons may result from an increase of excitatory drive onto these neurons, enhanced intrinsic excitability, a reduction of inhibitory drive onto these cells, or any combination of these. To examine the possibility that excitatory drive onto L2/3 PYR neurons increases after MD, we assayed the connectivity strength and laminar distribution of presynaptic excitatory inputs onto L2/3 PYR neurons in binocular cortex in acute brain slices using laser scanning photo stimulation (LSPS) via glutamate uncaging[13] (Fig. 1d–f and Supplementary Fig. 1). In control mice, maps of excitatory laminar inputs to L2/3 PYR neurons were consistent with those shown in previously published studies[13,14], with most inputs from L4, L5a and L2/3 as well as some weak input from deeper layers (Fig. 1e, f). MD did not significantly alter the amplitudes of excitatory postsynaptic currents (EPSCs) resulting from stimulation of presynaptic neurons originating in any cortical layer (two-way ANOVA on ranks $P = 0.756$; Fig. 1e, f), indicating that excitatory inputs to L2/3 PYR neurons were not altered at this early stage of plasticity. Spatially restricted photostimulation activates between 50 and 100 neurons at each LSPS location[15], although most of these stimulated neurons are not connected to the neuron being recorded. Because of this, glutamate uncaging may also be used to measure aggregate excitatory synaptic input onto the target neuron by evaluating the number of EPSCs elicited per LSPS location; this measure was also not different between control and 1-day MD (Supplementary Fig. 1). Taken together, local circuit mapping data indicate that 1 day of MD does not significantly change the strength or number of excitatory inputs to L2/3 PYR neurons from any cortical layer. Consistent with a previous report[16], we also did not find any evidence for a significant change in intrinsic excitability of the L2/3 PYR neurons whose inputs we mapped (Supplementary Fig. 1g), nor did we find evidence for a change in resting membrane potential (control: −67.46 ± 1.5 mV, $n = 8$ cells from 3 animals; MD: −65.9 ± 1.4 mV, $n = 7$ cells from 4 animals; Mann–Whitney *U*-test $P = 0.73$).

A remaining possibility is that a decrease in local inhibition underlies the enhanced visual responsiveness of L2/3 PYR neurons we observe after MD. Fast-spiking, parvalbumin-positive basket inhibitory neurons, referred to as PV cells, are increasingly implicated in both critical-period and adult plasticity[5,17]. To measure the impact of 1-day MD on PV responses, we used *in vivo* two-photon imaging to target cell-attached recordings to PV cells expressing the red fluorescent protein tdTomato. Spike waveform analysis was used to verify the identity of recorded neurons (Fig. 2a); recordings were made in alert and urethane-anaesthetized mice. Notably, the effect of 1-day MD on evoked firing rates of PV cells was the opposite of what we found for PYR neurons: whereas PYR spike rates roughly doubled, PV spike rates were roughly reduced by half. In anaesthetized mice, responses to stimulation through the ipsilateral, open eye were reduced by 42% (Fig. 2b, c; control: 16.2 ± 2.0 Hz, MD: 9.5 ± 0.9 Hz; two-way repeated measures ANOVA taking into account the pairwise relationship between ipsilateral and contralateral eye responses recorded for the same cell, $P = 0.002$, followed by post-hoc comparison, Bonferroni-corrected $P = 0.02$), and responses to stimulation through the reopened deprived, contralateral eye were also reduced, in this case by 54% (control: 19.8 ± 2.4 Hz, MD: 9.2 ± 0.9 Hz; Bonferroni-corrected $P = 0.002$). Similarly, in alert mice, PV responses to stimulation through the open eye dropped by 58% relative to controls after 1-day MD (control: 14.8 ± 3.1 Hz, $n = 10$ cells from 8 animals; MD: 6.2 ± 0.9 Hz, $n = 10$ cells from 7 animals; Mann–Whitney *U*-test $P = 0.001$). These recordings show that MD induces a rapid and severe drop in PV cell firing rates. Importantly, this effect is present for both eyes: responses through either the open or formerly closed eye were reduced by roughly half.

To identify the cause of this rapid, binocular reduction in visually evoked firing rates of PV cells, we again turned to recordings in acute brain slices to measure intrinsic excitability and to map the connectivity strength and laminar position of presynaptic excitatory inputs to PV cells. PV cells expressing tdTomato were visually targeted, their fast-spiking firing patterns were confirmed, and these cells were filled with biocytin for post-hoc morphological analysis. We found no evidence for altered intrinsic excitability as a function of current injection after MD (Supplementary Fig. 2), nor did we detect a change in resting membrane potential (control: −65.4 ± 1.5 mV, $n = 7$ cells from 3 animals; MD: −64.1 ± 0.74 mV, $n = 7$ cells from 4 animals; Mann–Whitney *U*-test $P > 0.8$). However, glutamate uncaging revealed an ~70% reduction in excitatory drive from cortical layers 4 and upper layer 5 onto L2/3 PV cells after 1-day MD (Fig. 3). The frequency of evoked (Fig. 3b) and spontaneous (Fig. 3c, d) EPSCs were significantly reduced in PV cells after 1-day MD, whereas the amplitude of spontaneous EPSCs was unchanged (Fig. 3e), suggesting both a weakening and reduction of excitatory synaptic inputs onto PV cells occurring at these earliest stages of cortical plasticity.

Notably, the rapid binocular reduction of PV firing rates after MD is transient. When MD was extended to 3 days, PV responses to stimulation of the deprived, contralateral eye (measured after acutely opening the sutured lids) remained as weak as they were after 1-day MD, but

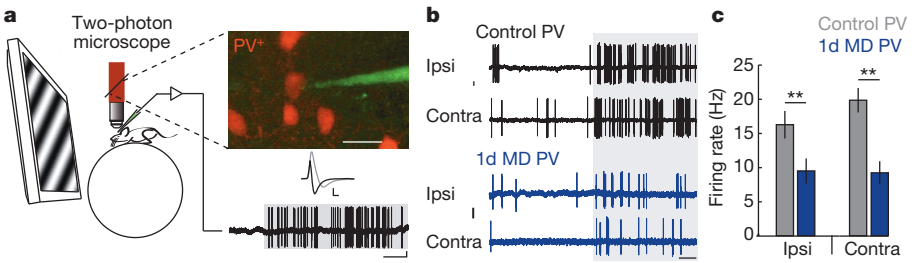

Figure 2 | L2/3 PV responsiveness to visual stimuli is reduced after 1-day MD. **a**, Cartoon of targeted recording in alert mice (left). Two-photon excitation (red beam) is used to visualize PV cells expressing tdTomato and recording pipette filled with Alexa dye (inset, 6 red PV cells; the pipette (green) is loose cell-attached to the PV cell in the centre of the image; scale bar, 20 μm). Spike waveform is used to verify targeting of fast-spiking PV cells (black trace; grey trace is a PYR neuron waveform for comparison; scale bar, 0.5 mV, 1 ms). Bottom, example PV response to visual stimulation (grey shading; scale bar, 1 mV, 500 ms). **b**, Example PV responses evoked by stimulation through either eye in control (black) and 1-day MD (blue) anaesthetized mice. Scale bar, 1 mV, 500 ms. **c**, Mean firing rate at optimal orientation (ipsilateral control: 14 mice, $n = 26$ cells; ipsilateral MD: 5 mice, $n = 18$ cells; contralateral control: 14 mice, $n = 26$ cells; contralateral MD: 5 mice, $n = 18$ cells). $^{**}P < 0.005$.

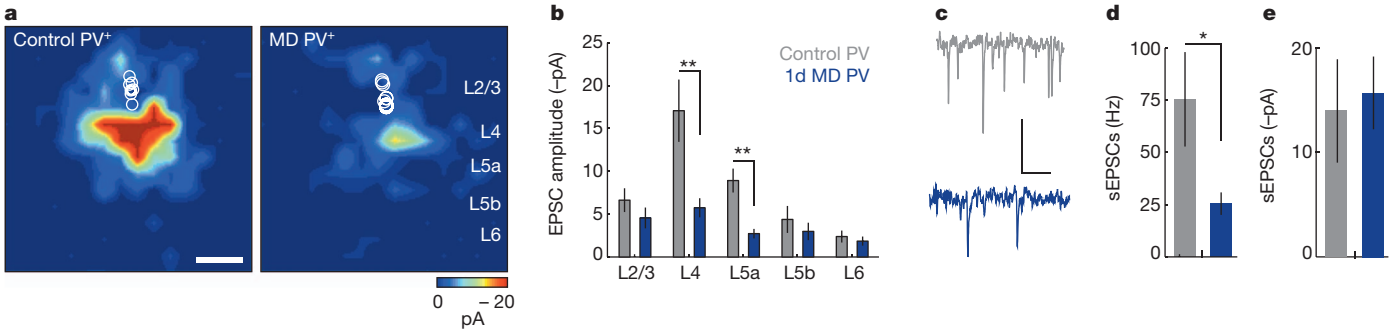

Figure 3 | L2/3 PV local circuit organization is altered after 1-day MD. **a**, *In vitro* LSPS aggregate excitatory input maps pooled across PV cells. Circles indicate soma location (control: 4 mice, $n = 7$ cells; MD: 4 mice, $n = 7$ cells). Scale bar, 200 μm. **b**, Mean laminar LSPS-evoked EPSC amplitude, same cells as **a**. $^{**}P < 0.007$. **c**, Example spontaneous EPSCs (sEPSCs). Scale bar, 20 pA, 100 ms. **d**, Mean sEPSC frequencies, same cells as **a**. $^{*}P < 0.05$. **e**, Mean sEPSC amplitude, same cells as **a**.

the strength of PV responses evoked by ipsilateral eye stimulation returned to normal (Supplementary Fig. 3). Thus, the rapid reduction in PV spike rates after 1-day MD is soon replaced by a restoration of normal PV responses to ipsilateral eye stimulation, which shifts PV ocular dominance towards the open eye.

A key question emerging from these findings is whether the transient binocular disinhibition following lid suture is necessary for subsequent shifts in excitatory ocular dominance. If so, one prediction is that maintaining inhibition after MD will prevent excitatory plasticity. To examine this we enhanced inhibition by injecting the use-dependent $GABA_A$ (γ-aminobutyric acid receptor-A) agonist diazepam into the ventricles of postnatal day (P)28 mice immediately after suturing the contralateral eye. Diazepam treatment effectively prevented the increase in ipsilateral eye excitatory firing rates seen after 1-day MD, but did not silence evoked activity (Supplementary Fig. 4a, b).

Cortical ocular dominance also was assayed 3 days after MD by imaging visually evoked fluorescent changes in L2/3 neurons bulk loaded with the calcium indicator Oregon Green BAPTA-1. Mice were exposed to 3 days of MD, and received intraventricular injections of either saline or diazepam for the first 2 days. Consistent with a role for disinhibition in ODP, intraventricular diazepam, but not vehicle, prevented shifts in cortical ocularity after MD (Supplementary Fig. 4c–h).

Because ODP is restricted to the critical period[9], a second prediction is that MD will not alter PV firing rates when performed thereafter. Supporting this we found no significant changes in evoked PV firing rates in monocularly deprived adult mice (age P42–45) relative to age-matched controls (Supplementary Fig. 5).

A third prediction is that ODP will be enhanced in older mice if PV spike rates are artificially reduced after MD. There is some precedent for this view[18]. In order to manipulate PV spike rates *in vivo*, we expressed hM_4D-inactivating G_i-coupled DREADD receptors[19–22] selectively in PV cells. Binding of the ligand clozapine N-oxide (CNO) to hM_4D receptors activates G-protein-coupled inwardly rectifying potassium channels, thereby reducing spike rates in target neurons for 9–12 h[23] (Supplementary Fig. 6). Three days of MD beginning at P35 does not normally shift cortical ocular dominance[9]. To determine whether a transient reduction in PV-mediated inhibition could reveal ODP in mice of this age, we tracked changes in cortical ocular dominance by imaging cortical responses to ipsilateral and contralateral eye stimulation longitudinally in mice expressing the genetically encoded calcium indicator GCaMP6 (ref. 24) in L2/3 of the binocular visual cortex. P35 mice given two injections of CNO at 12-h intervals immediately after lid suture (1 day of reduced PV inhibition) showed significant decreases in cortical responsiveness to the deprived eye without any significant

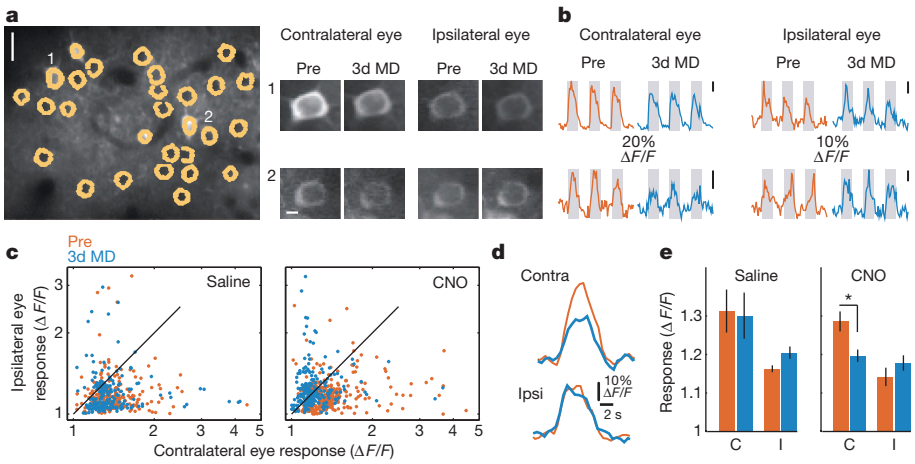

Figure 4 | Reducing PV-specific inhibition restores ODP after the closure of the critical period. **a**, Left, *In vivo* image of GCaMP6 expression, cells outlined in yellow. Scale bar, 20 μm. Right, individual images for cells labelled 1 and 2 of the average evoked fluorescence in response to visual stimuli presented independently to the contralateral and ipsilateral eye, before (pre) and 3 days after (3d) MD in a mouse expressing the hM_4D DREADD receptor specifically in PV cells, treated with CNO. Scale bar, 5 μm. **b**, Relative change in fluorescence before and after 3-day MD + CNO for cells 1 and 2 in panel **a** in response to visual stimulation (grey shading; 5-s duration). **c**, Log–log scatter plot of visually evoked fluorescence response for each cell (saline: $n = 242$ cells; CNO: $n = 327$ cells). Note the significant leftward shift after 3-day MD in mice treated with CNO (2-way ANOVA interaction, $P = 0.037$), but not those treated with saline (2-way ANOVA interaction, $P = 0.72$), indicating a reduced response to contralateral eye stimulation after 3-day MD. **d**, Longitudinal 'optical field potential' response (average value of all pixels in the entire imaging field, inclusive of neuropil) for the region in **a**. Note the decrease in response to contralateral eye stimulation after MD + CNO that is not seen for the ipsilateral eye. **e**, Mean 'optical field potential' response (saline: $n = 4$ mice; CNO: $n = 4$ mice). $^{*}P < 0.05$.

change in open, ipsilateral eye responses, whereas age-matched controls receiving similar injections of saline showed no changes in either measure (Fig. 4). Thus, a 24-h period of diminished PV firing is sufficient to restore juvenile-like ODP after the closure of the critical period.

The shift in ocular dominance after eye closure has been a long-standing paradigm for studying cortical plasticity. Mounting evidence implicates PV inhibitory neurons as regulators of this plasticity. How they do so, however, has remained incompletely understood. The data we present here define the role of PV cells in this process by showing that MD results in a rapid, but transient, reduction in PV-based inhibition, which restores PYR firing rates to pre-deprivation levels. Without this restoration of normal excitatory firing rates, subsequent competitive plasticity will not occur.

Our data and earlier papers examining the plasticity of the GABA population as a whole[25,26] or specifically PV cells[27] report that inhibitory responses ultimately shift towards the open eye after MD. Furthermore, there is a consensus that in non-deprived conditions, inhibitory cells are more binocular than excitatory cells in mice with normal GABA levels[25,27]. However, our data differ considerably from earlier studies on two fundamental issues: (1) the rate and direction of PV cell plasticity; and (2) the role of PV cell plasticity in excitatory ODP. Specifically, the possibility that PV cells become transiently, and paradoxically more responsive to deprived eye stimulation, thereby suppressing deprived-eye responses of excitatory neurons and shifting excitatory ocular dominance towards the open eye, was raised in a study that measured the ratio of the contralateral and ipsilateral eye responses in PV cells after brief MD[27]. In our measures of PV spike rates we did not find this paradoxical shift. Instead, we found that a rapid, transient and binocular reduction of fast-spiking inhibition permits, but does not instruct, synaptic competition among excitatory neurons. Our data redefine the role of fast-spiking inhibitory neurons as gating excitatory plasticity. It is the reduction of inhibition and the restoration of normal excitatory spike rates that permits competitive ODP to proceed on the basis of the relative strengths of the inputs of the two eyes.

Distinct mechanisms govern the influence of sensory experience on cortical plasticity early in life, in the form of passive sensory exposure, and in adulthood, in the form of reinforced associative learning[28]. The earliest stages of reinforced associative learning in primary sensory cortices appear to involve an active inhibition of PV inhibitory neurons via cholinergic activation of layer 1 interneurons[17,29]. Notably, our results indicate that a similar strategy—a reduction in PV cell firing rates and disinhibition of upper layer excitatory neurons—is used during the initial stages of binocular plasticity in adolescence, although by a loss of excitatory drive onto the PV cells. Together, these observations indicate that pathways regulating cortical plasticity in the juvenile and adult cortex converge on a rapid reduction of PV cell activity.

METHODS SUMMARY

All *in vivo* recordings were conducted in accordance with procedures approved by the University of California Los Angeles Office for Protection of Research Subjects and the Chancellor's Animal Research Committee. For work using cortical slices, the Institutional Animal Care and Use Committee at the University of California, Irvine, approved all procedures.

Full Methods and any associated references are available in the online version of the paper.

Received 8 October 2012; accepted 17 July 2013.
Published online 25 August 2013.

1. Ko, H. *et al.* The emergence of functional microcircuits in visual cortex. *Nature* **496,** 96–100 (2013).
2. White, L. E. & Fitzpatrick, D. Vision and cortical map development. *Neuron* **56,** 327–338 (2007).
3. Wiesel, T. N. & Hubel, D. H. Single-cell responses in striate cortex of kittens deprived of vision in one eye. *J. Neurophysiol.* **26,** 1003–1017 (1963).
4. Levelt, C. N. & Hubener, M. Critical-period plasticity in the visual cortex. *Annu. Rev. Neurosci.* **35,** 309–330 (2012).
5. Hensch, T. K. Critical period plasticity in local cortical circuits. *Nature Rev. Neurosci.* **6,** 877–888 (2005).
6. Jiang, B., Huang, Z. J., Morales, B. & Kirkwood, A. Maturation of GABAergic transmission and the timing of plasticity in visual cortex. *Brain Res. Brain Res. Rev.* **50,** 126–133 (2005).
7. Fu, M. & Zuo, Y. Experience-dependent structural plasticity in the cortex. *Trends Neurosci.* **34,** 177–187 (2011).
8. Holtmaat, A. & Svoboda, K. Experience-dependent structural synaptic plasticity in the mammalian brain. *Nature Rev. Neurosci.* **10,** 647–658 (2009).
9. Gordon, J. A. & Stryker, M. P. Experience-dependent plasticity of binocular responses in the primary visual cortex of the mouse. *J. Neurosci.* **16,** 3274–3286 (1996).
10. Webber, A. L. & Wood, J. Amblyopia: prevalence, natural history, functional effects and treatment. *Clin. Exp. Optom.* **88,** 365–375 (2005).
11. Holmes, J. M. *et al.* Effect of age on response to amblyopia treatment in children. *Arch. Ophthalmol.* **129,** 1451–1457 (2011).
12. Kanonidou, E. Amblyopia: a mini review of the literature. *Int. Ophthalmol.* **31,** 249–256 (2011).
13. Shepherd, G. M. & Svoboda, K. Laminar and columnar organization of ascending excitatory projections to layer 2/3 pyramidal neurons in rat barrel cortex. *J. Neurosci.* **25,** 5670–5679 (2005).
14. Yoshimura, Y. & Callaway, E. M. Fine-scale specificity of cortical networks depends on inhibitory cell type and connectivity. *Nature Neurosci.* **8,** 1552–1559 (2005).
15. Weiler, N., Wood, L., Yu, J., Solla, S. A. & Shepherd, G. M. Top-down laminar organization of the excitatory network in motor cortex. *Nature Neurosci.* **11,** 360–366 (2008).
16. Lambo, M. E. & Turrigiano, G. G. Synaptic and intrinsic homeostatic mechanisms cooperate to increase L2/3 pyramidal neuron excitability during a late phase of critical period plasticity. *J. Neurosci.* **33,** 8810–8819 (2013).
17. Letzkus, J. J. *et al.* A disinhibitory microcircuit for associative fear learning in the auditory cortex. *Nature* **480,** 331–335 (2011).
18. Harauzov, A. *et al.* Reducing intracortical inhibition in the adult visual cortex promotes ocular dominance plasticity. *J. Neurosci.* **30,** 361–371 (2010).
19. Ferguson, S. M. *et al.* Transient neuronal inhibition reveals opposing roles of indirect and direct pathways in sensitization. *Nature Neurosci.* **14,** 22–24 (2011).
20. Armbruster, B. N., Li, X., Pausch, M. H., Herlitze, S. & Roth, B. L. Evolving the lock to fit the key to create a family of G protein-coupled receptors potently activated by an inert ligand. *Proc. Natl Acad. Sci. USA* **104,** 5163–5168 (2007).
21. Dong, S., Allen, J. A., Farrell, M. & Roth, B. L. A chemical-genetic approach for precise spatio-temporal control of cellular signaling. *Mol. Biosyst.* **6,** 1376–1380 (2010).
22. Li, H. *et al.* Experience-dependent modification of a central amygdala fear circuit. *Nature Neurosci.* **16,** 332–339 (2013).
23. Alexander, G. M. *et al.* Remote control of neuronal activity in transgenic mice expressing evolved G protein-coupled receptors. *Neuron* **63,** 27–39 (2009).
24. Chen, T.-W. *et al.* Ultrasensitive fluorescent proteins for imaging neuronal activity. *Nature* **499,** 295–300 (2013).
25. Kameyama, K. *et al.* Difference in binocularity and ocular dominance plasticity between GABAergic and excitatory cortical neurons. *J. Neurosci.* **30,** 1551–1559 (2010).
26. Gandhi, S. P., Yanagawa, Y. & Stryker, M. P. Delayed plasticity of inhibitory neurons in developing visual cortex. *Proc. Natl Acad. Sci. USA* **105,** 16797–16802 (2008).
27. Yazaki-Sugiyama, Y., Kang, S., Cateau, H., Fukai, T. & Hensch, T. K. Bidirectional plasticity in fast-spiking GABA circuits by visual experience. *Nature* **462,** 218–221 (2009).
28. de Villers-Sidani, E. & Merzenich, M. M. Lifelong plasticity in the rat auditory cortex: basic mechanisms and role of sensory experience. *Prog. Brain Res.* **191,** 119–131 (2011).
29. Froemke, R. C., Merzenich, M. M. & Schreiner, C. E. A synaptic memory trace for cortical receptive field plasticity. *Nature* **450,** 425–429 (2007).

Supplementary Information is available in the online version of the paper.

Acknowledgements We thank S. Smith, W. Thompson, K. Miller and M. P. Stryker for comments on earlier versions of this manuscript, Y. Shi for help with software, Z. Nenadic for analytical suggestions, D. Ringach for help with GCaMP6 analysis and Z. J. Huang for useful discussions. This work was funded by grants from the US National Eye Institute (EY016052) to J.T.T., and the US National Institute of Neurological Disorders and Stroke (NS078434) and a NARSAD Young Investigator Grant to X.X.

Author Contributions S.J.K. and E.T. performed the *in vivo* awake and anaesthetized recordings. S.J.K. performed the diazepam/OGB-1 experiments. E.T. performed the DREADD/GCamp6 experiments. N.D.O. and T.I. performed the glutamate uncaging experiments. X.X. oversaw the glutamate uncaging experiments. J.T.T. oversaw all aspects of the project. S.J.K., N.D.O., X.X. and J.T.T. wrote the manuscript and prepared the figures.

Author Information Reprints and permissions information is available at www.nature.com/reprints. The authors declare no competing financial interests. Readers are welcome to comment on the online version of the paper. Correspondence and requests for materials should be addressed to X.X. (xiangmix@uci.edu) or J.T.T. (joshua.trachtenberg@gmail.com).

METHODS

All *in vivo* recordings were conducted in accordance with procedures approved by the University of California Los Angeles Office for Protection of Research Subjects and the Chancellor's Animal Research Committee. For work using cortical slices, the Institutional Animal Care and Use Committee at the University of California, Irvine, approved all procedures. To genetically label PV neurons, PV-IRES-cre knock-in female mice (Jackson Laboratories, stock no. 008069, generated by S. Arbor, FMI) were crossed with male tdTomato reporter knock-in mice directly received from Jackson Laboratory (Jackson Laboratories, stock no. 007905, 'Ai9', generated by H. Zeng, Allen Brain Institute). All experimental mice were hemizygous for both transgenes (PV-Cre:Ai9). Homozygous PV-IRES-cre mice used for the above breeding were all from a F_1 cross of a male and female directly received from Jackson Laboratory. Mice (male and female) were randomly assigned to either control or MD treatment groups. Sample sizes were chosen using a target power of 0.8. For cases in which analysis included a subjective component, analysis was done blind to experimental group as noted below. MD was performed under isoflurane/oxygen anaesthesia (3% induction and 2% maintenance isoflurane), antibacterial ointment applied to eyes, lid margins trimmed and one mattress suture (silk 6-O) was used to bind the upper and lower lids. In the case of 1-day MD alert recording experiments, lid margins were not trimmed to facilitate reopening. Any mice showing signs of eye infection or lid separation were removed from the study.

Electrophysiological recordings in alert mice. We followed the protocol outlined in ref. 30. To habituate mice to head restraint, mice were handled on the first day of training by repeatedly picking them up. On the second day, a metal bar later used to restrain the animal was fixed to the mouse's skull using dental acrylic. After a minimum of 2 days recovery, mice were placed on a floating styrofoam ball, head fixed and allowed to run for two 10-min sessions with a 10-min break in between. This was repeated daily, without the 10-min break, until mice showed signs of controlled navigation, including smooth transitions between running, walking, grooming and balancing without motion. Typically 2 days of head restraint atop the spherical treadmill was sufficient. On the day of recording, a 2-mm diameter craniotomy was made directly over the binocular zone of the primary visual cortex. Craniotomy placement and *in vivo* electrophysiology were performed as detailed in ref. 31. Craniotomies were centred 3 mm lateral of the sagittal suture and 1 mm rostral of the lambdoid suture. All experimental animals contained neurons that were driven by both the ipsilateral and contralateral eye in the recording zone. We refer to all non-fast spiking neurons (narrow-width action potentials[2]) as excitatory pyramidal neurons, although we do not rule out the possibility that up to 10% of the neurons are inhibitory neurons. Treadmill motion was monitored by measuring intensity changes in the reflectance of a red laser beam (Keyence Corporation, part no. LV-N11MN and LV-NH32) focused on the styrofoam ball. Electrophysiological signals were acquired in cell-attached configuration using a Multiclamp 700B amplifier (Molecular Devices) in current-clamp mode, digitized (PCI-6229M, National Instruments) at a sample rate of 10 kHz and low-pass filtered at 6 kHz. This method of recording is ideally suited to measuring changes in firing rates because there is not an inherent sampling bias for more active neurons, a bias that is present in other techniques that depend on isolating single units from multiunit activity.

Electrophysiological recordings in urethane anaesthetized mice. We followed the protocol outlined in ref. 31.

Visual stimulation and analysis of *in vivo* electrophysiology. To measure evoked firing rate at the preferred orientation, full-field drifting square wave gratings were presented at full contrast at 6 orientations spaced 30° apart at two directions of motion (12 orientations), using custom software developed with Psychtoolbox in Matlab. A 40-cm-width LCD monitor was placed 25 cm directly in front of alert or urethane-anaesthetized mice[31], tangent to the animal's gaze. Each stimulus was presented for 3 s, followed by a grey screen of equal duration. Stimulus orientations and direction were randomized. Varying spatial frequencies (0.02 and 0.04 cycles per degree) and temporal frequencies (1–2 Hz) were tested, and optimal stimulation was then shown for 4–9 trials. In awake recordings, periods of grooming and any periods >60 s in which there was no treadmill motion detected were excluded from further analysis. Evoked rates were computed as the spike rate for a given orientation, averaged across the 3-s stimulation window and across 4–9 trials, and were baseline-subtracted. Baseline was defined as the average spike rate in response to all grey screen presentations. Evoked rate at the preferred orientation is reported. To analyse spike shape, the first 50 spike waveforms were averaged for a given cell. The 10–90% rising and falling slope, and peak (P1) and nadir (P2) amplitudes were calculated from the average trace.

Eye shuttering. Eye shuttering was accomplished by manually placing an occluding device 5 mm in front of the eye. The occluding device was constructed of flexible light-blocking material (1.2 × 1.5 cm) mounted to a vertical post, 5 mm in diameter, coupled to a magnetic base that was released and alternately placed in front of either eye as indicated by the interleaved trial schedule.

Visual cortical slice preparations. The littermates of double-transgenic mice (PV-Cre:Ai9, aged P28–P29) were used for either control or the treatment of 24-h MD. For each experimental day, a pair of the control and MD-treated animals was deeply anaesthetized using pentobarbital sodium (100 mg kg^{-1}, intraperitoneally), transcardially perfused with chilled oxygenated artificial cerebrospinal fluid (ACSF), rapidly decapitated and brain extracted. Coronal sections of 400 μm were cut from primary visual cortex (V1) with a vibratome (VT1200S, Leica Systems) in sucrose containing ACSF (in mM: 85 NaCl, 75 sucrose, 2.5 KCl, 25 glucose, 1.25 NaH_2PO_4, 4 $MgCl_2$, 0.5 $CaCl_2$ and 24 $NaHCO_3$). For animals having undergone MD, sections were taken exclusively from the hemisphere contralateral to the deprived eye. Slices were incubated for at least 30 min in sucrose containing ACSF at 32 °C before being transferred into slice recording chambers with normal ACSF (in mM: 126 NaCl, 2.5 KCl, 26 $NaHCO_3$, 2 $CaCl_2$, 2 $MgCl_2$, 1.25 NaH_2PO_4 and 10 glucose). Throughout the cutting, incubation and recording, the solutions were continuously supplied with 95% O_2–5% CO_2.

Electrophysiology and LSPS. Electrophysiological recordings and photostimulation were performed as in ref. 32. Whole-cell recordings were performed under a DIC/fluorescent Olympus microscope (BX51WI). Oxygenated ACSF at room temperature (25° C) was perfused into the slice recording chamber through a custom-designed flow system driven by pressurized 95% O_2–5% CO_2 (3 PSI) at roughly 2 ml min^{-1}. Slices were examined under a 4× objective for proper targeting of either L2/3 pyramidal neurons or tdTomato-expressing PV-positive interneurons within binocular regions of mouse V1 using landmarks defined in ref. 33. To target whole-cell recordings, cells were visualized at high magnification (60× objective, 0.9 NA; LUMPlanFl/IR, Olympus). Cell bodies of recorded neurons were at least 50 μm below the surface of the slice. Patch pipettes (4–6 MΩ resistance) made of borosilicate glass were filled with an internal solution containing (in mM) 126 K-gluconate, 4 KCl, 10 HEPES, 4 ATP-Mg, 0.3 GTP-Na and 10 phosphocreatine (pH 7.2, 300 mOsm). Electrodes also contained 0.1% biocytin for post-hoc cell labelling and further morphological identification. Once stable whole-cell recordings were achieved with good access resistance (usually <20 MΩ), basic electrophysiological properties were examined through hyperpolarizing and depolarizing current injections. Electrophysiological data were acquired with a Multiclamp 700B amplifier (Molecular Devices), data acquisition boards (models PCI MIO 16E-4 and 6713, National Instruments) and custom-modified version of Ephus software[34] (Ephus, available at https://openwiki.janelia.org/). Data were digitized at 10 kHz.

PV-positive inhibitory neurons were targeted on the basis of RFP expression and verified by fast-spiking patterns from current injections and large basket cell morphology. Excitatory neurons were selected on the basis of their pyramidal somata detected under DIC, were RFP negative and showed adapting spiking patterns to suprathreshold intrasomatic current injections. Final cell type classification was determined by the combined characterization of RFP expression, electrophysiological and morphological properties of the recorded cells.

The LSPS procedures were similar to those described in refs 13 and 35. LSPS was performed through a 4× objective lens. Stock solution of MNI-caged-L-glutamate (Tocris Bioscience) was added to 20 ml ACSF for a concentration of 0.2 mM caged glutamate. The cortical slice image, acquired through the 4× objective, was visualized using a high-resolution digital CCD camera, and this image, in turn, was used to guide and register photostimulation sites. Two-millisecond duration, 20-mW pulses from a 350 nm UV laser (DPSS Lasers) were delivered to the sample, controlled via an electro-optical modulator and a mechanical shutter. Focal laser spots approximated a Gaussian profile with a lateral width of 100 μm. Under our experimental conditions, LSPS-evoked action potentials were recorded from stimulation locations within 124 μm (96 ± 28 μm, $n = 12$) of targeted somata and occurred within 150 ms after photostimulation. Synaptic currents in patched neurons were detected under voltage clamp. By systematically surveying synaptic inputs from hundreds of different sites across a large cortical region, aggregate synaptic input maps were generated for individual neurons. For our mapping experiments, a standard stimulus grid (16 × 16 stimulation sites, 65 μm^2 spacing) was used to tessellate V1 from pia to white matter. The LSPS site spacing was empirically determined to capture the smallest predicted distance in which photostimulation differentially activates adjacent neurons. Glutamate uncaging was delivered sequentially in a nonraster, nonrandom sequence, following a 'shifting-X' pattern designed to avoid revisiting the vicinity of recently stimulated sites[36].

Because glutamate uncaging activates both excitatory and inhibitory neurons, we empirically determined the excitatory and inhibitory reversal potentials in L2/3 pyramidal cells to properly isolate EPSCs and IPSCs. In a subset of experiments, L2/3 neurons were voltage clamped at a range of holding potentials from −90 mV to 5 mV, and GABA uncaging (0.1 mM, Invitrogen) was performed by delivering brief ultraviolet flashes (1 ms, 20 mW) to the perisomatic regions of targeted cells to determine the GABAergic reversal potential on the basis of voltage–current relationships. The average GABAergic reversal potential ranged from −69 mV to

−71 mV, and we therefore voltage clamped the targeted pyramidal cells at −70 mV to determine LSPS and spontaneously evoked EPSCs.

Laminar circuit input analysis. Photostimulation induces two forms of excitatory responses: (1) those that result from direct activation of the recorded neuron's glutamate receptors; and (2) synaptically mediated responses (EPSCs) resulting from the suprathreshold activation of presynaptic excitatory neurons. Responses that occur within 10 ms of laser pulse onset were considered direct; these responses exhibited a distinct shape and occurred immediately after glutamate uncaging. Synaptic currents with such short latencies are not possible because they would have to occur before the generation of action potentials in photostimulated neurons. Therefore, direct responses need to be excluded from local synaptic input analysis. To check for any systematic differences across treatment conditions, the spatial extent and frequency of action potentials elicited in response to direct stimulation was determined in a subset of the experiments by performing whole-cell recordings in current-clamp mode using an 8 × 8 mapping grid. Direct stimulation was found to be similar for control and MD; direct responses were restricted to within approximately 100 μm of the recorded soma (control: 86 ± 22 μm, $n = 7$ cells; MD: 106 ± 34 μm, $n = 5$ cells) and were limited to less than 1.5 action potentials averaged across trials (control: 1 ± 0, $n = 7$ cells; MD: 1.2 ± 0.2 $n = 5$ cells). At some locations, synaptic responses were over-riding on relatively small direct responses (see Supplementary Fig. 1d); such responses were identified and included in synaptic input analysis.

For data map analysis, we implemented the approach for detection and extraction of photostimulation-evoked postsynaptic current responses described in ref. 37. LSPS-evoked EPSCs were quantified across the 16 × 16 mapping grid for each cell, and 2 to 4 individual maps were averaged per recorded cell, reducing the likelihood of incorporating noise events in the analysis window (150 ms). Averaged maps were then analysed using the 4× DIC image to bin responses according to laminar cytoarchitectonic landmarks. Synaptic events were binned from locations spanning ±195 μm tangential to the targeted soma location and from the top of layer 2/3 to the bottom of layer 6 across the radial vector. Data were plotted as either the average integrated EPSCs amplitude per pixel location or the number of EPSCs detected per pixel location.

Morphological examination and cell-type Identification. The morphology of each recorded neuron was determined using post-hoc staining. In brief, brain slices were fixed in 4% paraformaldehyde and transferred to 30% sucrose solution in PBS. Neurons filled with biocytin during recordings were labelled with Alexa Fluor 488-conjugated streptavidin (1:500 dilution; Jackson ImmunoResearch). Slices were also stained for 4′-6-diamidino-2-phenylindole (DAPI) (Sigma-Aldrich) to identify laminar boundaries. Cell morphology, DAPI labelling and RFP expression were visualized using an Olympus BX 61 epifluorescent microscope and MetaMorph imaging suite (Molecular Devices).

Calcium imaging using Oregon Green BAPTA-1. Mice were anaesthetized with urethane and core body temperature was maintained using a closed loop heated plate and a rectal temperature sensor. Neurons in L2/3 of the primary visual cortex were bulk labelled with the calcium indicator Oregon Green BAPTA-1 (OGB), and changes in fluorescence intensity were imaged as described in refs 38 and 39. Dye was injected at 2–3 positions to ensure labelling within the binocular region. Three days before calcium imaging, mice were randomly assigned to one of three groups: control, MD or MD plus diazepam (pharmaceutical grade; Hospira) treatment. Intraventricular injections (1.5 μl volume) of either vehicle (50% propylene glycol/50% saline) or diazepam (2 mg ml^{-1} in 50% propylene glycol) were performed in isoflurane/oxygen-anaesthetized mice (3% induction, 1–2% maintenance) using a Hamilton needle (30 gauge) and syringe (5 μl capacity) mounted to a manipulator (MP285, Sutter). The injection depth was 2.25 mm; entry site was 0.5 mm lateral from midline and immediately anterior of bregma (primary motor cortex). Two injections were made, the initial injection was made at the time of MD on the same side as the MD, and the second injection was made on the other hemisphere 24–28 h after the initial injection. Coordinates were verified before the experiment in three test animals by injecting 1,1′-dioctadecyl-3,3,3′,3′-tetramethylindocarbocyanine percholate (DiI; 0.5 μl) and perfusing mice 1 day later. Brains were then sectioned, slices were visualized under epifluorescence and it was determined that DiI was specifically localized to ventricles using the above coordinates.

Expression of GCaMP6 and hM$_4$D DREADD receptors. PV-Cre mice were anaesthetized with isoflurane and core body temperature maintained as above. The scalp was retracted and a small burr hole was drilled over the left occipital pole overlying the binocular zone of primary visual cortex. GCaMP6 (ref. 24; UPenn Vector Core: AAV-1-PV2824; generously supplied by the GENIE Project, Janelia Farm Research Campus, Howard Hughes Medical Institute) and Cre-dependent hM$_4$D DREADD receptors[19,20,40] (UNC Vector Core: AAV-hSyn-DIO-hM$_4$D(G$_i$)-mCherry) were expressed in cortical neurons using adeno-associated virus (AAV). Notably, hM$_4$D receptors were only expressed in PV-Cre cells. AAV-GCaMP6 and AAV-hM$_4$D were mixed at a 1:1 ratio (injected concentration 2.5×10^{11} genome copies per ml) and loaded into a glass micropipette. The pipette was slowly inserted into the cortex and five injections were made, one each at 350, 300, 250, 200 and 150 μm below the pial surface along a single injection tract. AAV was pressure injected at each site using a PicoSpritzer: 30 puffs at 10 pounds per square inch and 10-ms duration was used at each site. Total volume injected across all five sites was roughly 0.5 μl. The scalp was then sutured shut over the burr hole and the mouse was left for 2 weeks to enable high GCaMP6 and hM$_4$D expression. Thereafter, a craniotomy was performed to expose a 2.5-mm-diameter region of the brain centred on binocular visual cortex, and the craniotomy was sealed with a no. 1 coverglass as described previously[41].

Visual stimulation and data acquisition. To evoke responses in labelled neurons, visual stimuli were presented based on the methods of ref. 42. Neural responses to stimulation of either eye were assessed using full-field drifting square wave gratings presented at full contrast at six orientations spaced 30° apart at two directions of motion (12 orientations, temporal frequency of 2 Hz, 0.04 cycles per degree) every 11 s for a duration of 5 s preceded by a grey screen for a duration of 6 s. During the stimulation time, randomly chosen grating orientations changed every 0.4 s. Four stimulus repetitions were presented and interleaved between eye stimulation. Image sequences (256 × 256 pixels, covering a field of view of 130 × 130 μm) were acquired at 2.05 Hz at a depth of 180–300 μm below the pia surface using ScanImage software[43]. Fields of view that contained no or unevenly distributed responses to ipsilateral eye stimulation, an indication that the imaged position was outside or at the border of the binocular zone, were excluded from further analysis. Neurons were distinguished from astrocytes using sulforhodamine coinjection[44]. During OGB and GCaMP6 imaging, red (semrock filter: 583/22) and green (semrock filter: 510/84) emissions were separated (semrock dichroic: FF568) and detected simultaneously using two photomultiplier tubes (PMTs; Hamamatsu R3896). OGB was excited at wavelength of 870 nm. GCaMP6 was excited at 940 nm. When imaging OGB, PV interneurons were subsequently identified and excluded from analysis by switching the excitation wavelength to 960 nm. When imaging GCaMP6, PV interneurons were identified by their emission in the red channel. To facilitate defining the stimulus onset for each cell, output from a photodiode affixed to the presentation monitor was digitized simultaneously with the output from the PMTs.

For GCaMP6/hM$_4$D-expressing mice, images of cell responses to visual stimulation were first obtained on P35. Immediately thereafter the lid margins to the contralateral eye were sutured shut for 3 days. During the first day of lid suture mice either received two intraperitoneal injections, spaced 12 h apart of either saline or CNO (5 mg kg^{-1} dissolved in 0.9% sterile saline). On P38, the lid margins were reopened and cortical responses to visual stimulation through both the ipsilateral and contralateral eyes were assessed. Distributions of ipsilateral and contralateral response strength after MD in both conditions were compared to those obtained from baseline images.

Data analysis. A semiautomatic custom-written routine (Matlab) was used to identify the outlines of individual OGB-loaded cells[38]. In brief, an average image was generated from the acquired time series and the x,y spatial position of a given cell was seeded by the user, blind to experimental condition. The spatial location of the cell border was then calculated based on identifying a contiguous region having a > 1.1-fold intensity above the local average. Local average and maximum cell size was bounded by a square area R × R centred on the user defined seed pixel, where R = 25 μm. For GCaMP6 imaging, where labelled neurons have a donut appearance, we used a separate method for segmenting neurons. In brief, after manual selection of the cells to be studied, a deformable snake was used to track their individual boundaries[45], along with morphological dilation[46] to define the region of interest for each cell. For both OGB and GCaMP6 images, the pixels within each cell's region of interest were averaged to generate a single time course of fluorescent intensity for each individual cell. Response amplitude was computed from 8–12 stimulus repetitions as the first 5 frames immediately following the frame of stimulus onset divided by the average of the 6 frames preceding stimulus onset. The frame of stimulus onset was defined independently for each cell. Cells were considered responsive if the calcium transients to any of the orientation stimuli were significantly different from the baseline (ANOVA at $P < 0.01$). An ocular dominance score was calculated for all responsive cells (excluding identified PV interneurons and astrocytes) as 1 minus the ratio of the ipsilateral eye response divided by the summed response of both eyes. For each animal, a histogram of ocular dominance scores was generated and the contralateral bias index was calculated as in ref. 9, using the following formula: $((n_1-n_7)+(2/3)(n_2-n_6)+(1/3)(n_3-n_5)+N)/(2N)$, in which N = total number of responsive cells and n_x is the number of cells with ocular dominance scores equal to x.

Statistical analyses and bar graphs. All data are reported as mean ± standard error of the mean (s.e.m.). When comparing two independent groups, normally distributed data were analysed using a Student's t-test, in the case data were not normally distributed a Mann–Whitney U-test was used. In the case more than

two groups were compared and data were normally distributed, an ANOVA was performed as indicated in main text and followed by post-hoc comparisons when justified (alpha set to 0.05). Post-hoc P values were corrected for multiple comparisons as indicated. Bonferroni correction was used unless data had unequal variances (assessed by the Levene statistic), in that case Tamhane correction was used. In all cases, sample size n was defined as cell number, except in the case of comparing the contralateral bias index across treatments and GCaMP6 'optical field potential', where n was defined as animal number.

30. Dombeck, D. A., Khabbaz, A. N., Collman, F., Adelman, T. L. & Tank, D. W. Imaging large-scale neural activity with cellular resolution in awake, mobile mice. *Neuron* **56,** 43–57 (2007).
31. Kuhlman, S. J., Tring, E. & Trachtenberg, J. T. Fast-spiking interneurons have an initial orientation bias that is lost with vision. *Nature Neurosci.* **14,** 1121–1123 (2011).
32. Xu, X., Olivas, N. D., Levi, R., Ikrar, T. & Nenadic, Z. High precision and fast functional mapping of cortical circuitry through a novel combination of voltage sensitive dye imaging and laser scanning photostimulation. *J. Neurophysiol.* **103,** 2301–2312 (2010).
33. Antonini, A., Fagiolini, M. & Stryker, M. P. Anatomical correlates of functional plasticity in mouse visual cortex. *J. Neurosci.* **19,** 4388–4406 (1999).
34. Suter, B. A. *et al. Ephus*: multipurpose data acquisition software for neuroscience experiments. *Front. Neural Circuits* **4,** 100 (2010).
35. Hooks, B. M. *et al.* Laminar analysis of excitatory local circuits in vibrissal motor and sensory cortical areas. *PLoS Biol.* **9,** e1000572 (2011).
36. Shepherd, G. M., Pologruto, T. A. & Svoboda, K. Circuit analysis of experience-dependent plasticity in the developing rat barrel cortex. *Neuron* **38,** 277–289 (2003).
37. Shi, Y., Nenadic, Z. & Xu, X. Novel use of matched filtering for synaptic event detection and extraction. *PLoS ONE* **5,** e15517 (2010).
38. Gdalyahu, A. *et al.* Associative fear learning enhances sparse network coding in primary sensory cortex. *Neuron* **75,** 121–132 (2012).
39. Stosiek, C., Garaschuk, O., Holthoff, K. & Konnerth, A. *In vivo* two-photon calcium imaging of neuronal networks. *Proc. Natl Acad. Sci. USA* **100,** 7319–7324 (2003).
40. Rogan, S. C. & Roth, B. L. Remote control of neuronal signaling. *Pharmacol. Rev.* **63,** 291–315 (2011).
41. Holtmaat, A. *et al.* Long-term, high-resolution imaging in the mouse neocortex through a chronic cranial window. *Nature Protocols* **4,** 1128–1144 (2009).
42. Mrsic-Flogel, T. D. *et al.* Homeostatic regulation of eye-specific responses in visual cortex during ocular dominance plasticity. *Neuron* **54,** 961–972 (2007).
43. Pologruto, T. A., Sabatini, B. L. & Svoboda, K. ScanImage: flexible software for operating laser scanning microscopes. *Biomed. Eng. Online* **2,** 13 (2003).
44. Nimmerjahn, A., Kirchhoff, F., Kerr, J. N. & Helmchen, F. Sulforhodamine 101 as a specific marker of astroglia in the neocortex *in vivo*. *Nature Methods* **1,** 31–37 (2004).
45. Xu, C. & Prince, J. L. Snakes, shapes, and gradient vector flow. *IEEE Trans. Image Process.* **7,** 359–369 (1998).
46. Shih, F. Y. *Image Processing and Mathematical Morphology: Fundamentals and Applications* (CRC, 2009).